

High performance NbN nanowire superconducting single photon detectors fabricated on MgO substrates

F. Marsili
francesco.marsili@epfl.ch

D. Bitauld
A. Fiore

*Ecole Polytechnique Fédérale de Lausanne (EPFL), Institute of Photonics and Quantum
Electronics (IPEQ), Station 3, CH-1015 Lausanne, Switzerland*

A. Gaggero
F. Mattioli
R. Leoni

*Istituto di Fotonica e Nanotecnologie (IFN), CNR, via del Cineto Romano 42, 00156 Roma,
Italy*

M. Benkahoul
F. Lévy

*Ecole Polytechnique Fédérale de Lausanne (EPFL), Institute of Complex Matter Physics
(IPMC), Station 3, CH-1015 Lausanne, Switzerland*

Abstract: We demonstrate high-performance nanowire superconducting single photon detectors (SSPDs) on ultrathin NbN films grown at a temperature compatible with monolithic integration. NbN films ranging from 150nm to 3nm in thickness were deposited by dc magnetron sputtering on MgO substrates at 400°C. The superconducting properties of NbN films were optimized studying the effects of deposition parameters on film properties. SSPDs were fabricated on high quality NbN films of different thickness (7 to 3nm) deposited under optimal conditions. Electrical and optical characterizations were performed on the SSPDs. The highest QE value measured at 4.2K is 20% at 1300nm.

© 2018 Optical Society of America

OCIS codes: (000.0000) General.

References and links

1. H. Takesue, S. W. Nam, Q. Zhang, R. H. Hadfield, T. Honjo, K. Tamaki, and Y. Yamamoto, “Quantum key distribution over a 40-dB channel loss using superconducting single-photon detectors,” *Nature Phot.* **1**(6), 343–348 (2007).
2. G. N. Gol’tsman, O. Okunev, G. Chulkova, A. Lipatov, A. Semenov, K. Smirnov, B. Voronov, A. Dzardanov, C. Williams, and R. Sobolewski, “Picosecond superconducting single-photon optical detector,” *Appl. Phys. Lett.* **79**(6), 705–707 (2001).
3. A. Korneev, V. Matvienko, O. Minaeva, I. Milostnaya, I. Rubtsova, G. Chulkova, K. Smirnov, V. Voronov, G. Gol’tsman, W. Slysz, A. Pearlman, A. Verevkin, and R. Sobolewski, “Quantum efficiency and noise equivalent power of nanostructured, NbN, single-photon detectors in the wavelength range from visible to infrared,” *IEEE Transactions on Applied Superconductivity* **15**(2 PART I), 571–574 (2005).
4. K. M. Rosfjord, J. K. W. Yang, E. A. Dauler, A. J. Kerman, V. Anant, B. M. Voronov, G. N. Gol’tsman, and K. K. Berggren, “Nanowire Single-photon detector with an integrated optical cavity and anti-reflection coating,” *Opt. Express* **14**(2), 527–534 (2006).

5. K. Iizuka, K. Matsumaru, T. Suzuki, H. Hirose, K. Suzuki, and H. Okamoto, "Arsenic-free GaAs substrate preparation and direct growth of GaAs/AlGaAs multiple quantum well without buffer layer," *Journal of Crystal Growth* **150**(1-4 pt 1), 13–17 (1995).
6. S. Miki, M. Fujiwara, M. Sasaki, and Z. Wang, "NbN superconducting single-photon detectors prepared on single-crystal MgO substrates," *IEEE Trans. Appl. Supercond.* **17**(2), 285–288 (2007).
7. D. D. Bacon, A. T. English, S. Nakahara, F. G. Peters, H. Schreiber, W. R. Sinclair, and R. B. van Dover, "PROPERTIES OF NbN THIN FILMS DEPOSITED ON AMBIENT TEMPERATURE SUBSTRATES," *J. Appl. Phys.* **54**(11), 6509–6516 (1983).
8. J. C. Villegier, L. Vieux-Rochaz, M. Goniche, P. Renard, and M. Vabre, "NbN TUNNEL JUNCTIONS," *IEEE Trans. Mag.* **21**(2), 498–504 (1984).
9. M. Benkahoul, E. Martinez, A. Karimi, R. Sanjinés, and F. Lévy, "Structural and mechanical properties of sputtered cubic and hexagonal NbN_x thin films," *Surf. Coat. Technol.* **180-181**, 178–183 (2004).
10. H. C. Jones, "Some properties of granular thin films of high-field superconductors," *Appl. Phys. Lett.* **27**(8), 471–473 (1975).
11. F. Mattioli, R. Leoni, A. Gaggero, M. G. Castellano, P. Carelli, F. Marsili, and A. Fiore, "Electrical characterization of superconducting single-photon detectors," *J. Appl. Phys.* **101**(5), 054,302 (2007).
12. W. J. Skocpol, M. R. Beasley, and M. Tinkham, "SELF-HEATING HOTSPOTS IN SUPERCONDUCTING THIN-FILM MICROBRIDGES," *J. Appl. Phys.* **45**(9), 4054–4066 (1974).
13. A. Verevkin, J. Zhang, R. Sobolewski, A. Lipatov, O. Okunev, G. Chulkova, A. Korneev, K. Smimov, G. N. Gol'tsman, and A. Semenov, "Detection efficiency of large-active-area NbN single-photon superconducting detectors in the ultraviolet to near-infrared range," *Appl. Phys. Lett.* **80**(25), 4687 (2002).
14. A. J. Miller, S. W. Nam, J. M. Martinis, and A. V. Sergienko, "Demonstration of a low-noise near-infrared photon counter with multiphoton discrimination," *Appl. Phys. Lett.* **83**(4), 791–793 (2003).

1. Introduction

High counting-rate detectors capable of efficient single photon sensing in the infrared region are needed for several applications in different fields, including high-bandwidth interplanetary optical communications, test of high-speed semiconductor circuits, quantum optics and quantum communications [1]. Nanowire superconducting single photon detectors (SSPDs) [2] are interesting candidates for these requirements. So far, high-sensitivity ultrafast SSPDs have been fabricated only on 4nm thick NbN films grown on sapphire substrates at high temperatures (typically 900°C) [3, 4]. This significantly limits the integration of SSPDs with advanced optical structures (e.g. waveguides and microcavities) and read-out electronics, typically realized on other substrates and not compatible with these deposition temperatures. For instance, high reflectivity DBR realized on GaAs do not withstand such temperatures due to As outgassing [5]. Very recently, fabrication of SSPDs on MgO at room temperature has been reported, but their quantum efficiency (QE) is very low [6]. In an effort to develop an exportable technology, we show that high performance NbN SSPDs can be implemented on different substrates (e.g. MgO) and at lower deposition temperatures ($\sim 400^\circ\text{C}$), which opens the way to monolithic integration.

2. Thin film deposition and device fabrication

NbN films ranging from 150nm to 3nm in thickness were deposited on epitaxial-quality single crystal MgO $< 100 >$ substrates by current controlled dc magnetron sputtering from a Nb target (5cm diameter, 99.95% purity) in a mixture of Ar (99.9997% purity) and N₂ (99.999% purity). The background pressure was in the low 10^{-7} torr range. The distance between target and substrate was fixed at the maximum allowed by our system (85mm) to maximize film uniformity. In order to control the thickness of ultrathin films, the deposition rate R was kept in the few Å/s range, which fixed the plasma current at $I_p = 250\text{mA}$. Low total pressures P_{tot} (in the few mtorr range) were used, resulting in power densities of the order of $10\text{W}/\text{cm}^2$. The high sputtering energy allowed to promote the growth of high quality NbN films at a substrate temperature as low as $T_S = 400^\circ\text{C}$. Following a well established procedure [7, 8], the superconducting properties of NbN films were optimized studying the effects of P_{tot} and composition of

reactive gas on film structural and electrical properties. For every P_{tot} the superconducting critical temperature T_C showed a maximum as a function of nitrogen partial pressure P_{N_2} , which was varied within the limits determined by the requirement to produce the NbN superconducting δ phase [9]. Decreasing P_{tot} improved the quality of NbN films: an increase in the maximum of T_C and a decrease in the superconducting transition width ΔT_C and Residual Resistivity Ratio (the ratio between the resistivity at 300K and at 20K, $RRR = \rho_{300K}/\rho_{20K}$) were observed. $P_{tot}=2.5$ mtorr, $P_{N_2}/P_{tot} = 33\%$, were found to be the optimal deposition parameters, resulting in a $T_C=16.1$ K, with a $\Delta T_C=60$ mK and an $RRR = 1$ for a 150nm thick film, which indicates that no intergrain voids were present [10]. Decreasing the thickness of films led to a slight degradation of their superconducting properties (Fig. 1), but the thinnest film ($t=3$ nm) still exhibited $T_C=8.6$ K, $\Delta T_C=0.9$ K and $RRR = 0.6$, proof of the excellent quality of our low-temperature deposition process. The crystallinity of the best films was characterized using X-ray diffraction: they showed a fcc, NaCl-type crystal structure, with a lattice constant $a_0 = 4.45\text{\AA}$, which agrees with reported results [7, 8]. From cross-sectional transmission electron microscopy (TEM) investigation it was determined that NbN grows on MgO substrate without any initial amorphous layers.

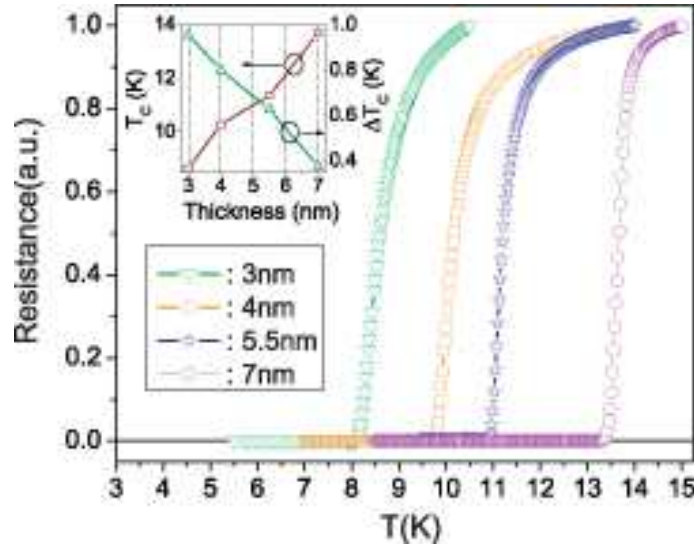


Fig. 1. Resistance vs temperature dependence of NbN films for four thicknesses: 7nm (circles), 5.5nm (stars), 4nm (squares) and 3nm (triangles). The deposition conditions were: $T_S = 400^\circ\text{C}$, $I_p = 250\text{mA}$, $P_{tot}=2.5$ mtorr, 33% N_2 , $R=3\text{\AA}/\text{s}$. Inset: T_C and ΔT_C vs. thickness (t). T_C vary from 13.7K ($\Delta T_C=0.4$ K) for $t=7$ nm to 8.6K ($\Delta T_C=0.9$ K) for $t=3$ nm.

SSPDs were fabricated on ultrathin NbN films deposited under optimal conditions on MgO by a two mask process using electron beam lithography (EBL) and reactive ion etching [11]. Detectors are $5 \times 5 \mu\text{m}^2$ in size, and composed of nanowires ranging from 60nm to 100nm in width (w), folded in a meander pattern with fill factors (f) ranging from 40% to 60%. The meanders are contacted through 70nm thick Au-Ti pads, patterned as a 50Ω coplanar transmission line. The same structures were fabricated on films of four different thicknesses (t): 7nm, 5.5nm, 4nm and 3nm. The thickness of NbN films was measured by AFM. T_C and ΔT_C of the patterned SSPD were found to be the same as those of the original NbN films, which confirms that the fabrication process does not affect their superconducting properties.

3. Measurements

The uniformity in width of the nanowires was verified by extensive scanning electron microscopy (SEM). To prevent charging effects, the devices were coated by a 10nm thick layer of OsO₄. This conductive coating, whose grain size is less than 1nm, allowed ultra-high resolution SEM imaging on the meanders. Fig. 2 shows an SEM image of a $w=100\text{nm}$, $f=40\%$ meander. Note that the contact pads on the two sides of the meander were also patterned with a low fill factor to reduce proximity effects during the EBL writing step. It was then possible to estimate the mean width variation as $\Delta w \sim 10\text{nm}$, which agrees with the results of electrical characterization on test structures [11].

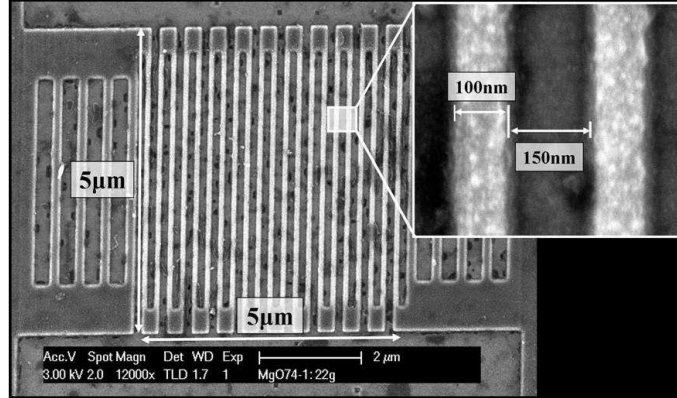


Fig. 2. Scanning electron microscope (SEM) image of an SSPD. The nanowire width is $w=100\text{nm}$, the fill factor is $f=40\%$. The inset shows an ultra-high resolution image of two stripes. The mean width variation was estimated to be $\Delta w \sim 10\text{nm}$.

Electrical and optical characterizations have been performed on the SSPDs. In total, 320 devices were tested, 80 for each of the four different film thicknesses of interest. For each chip, the best devices were first selected measuring their current-voltage (I-V) curves inside a cryogenic probe station (Janis). Electrical contact was realized by a cooled 50Ω microwave probe attached to a micromanipulator, and connected by a coaxial line to the room-temperature circuitry. The samples were DC biased using a low noise voltage source in series with a bias resistor R_B . I-V curves of our devices (Fig. 3) are typical for a superconducting one-dimensional bridge much longer than the thermal healing length ($\eta \sim 100\text{nm}$), at a temperature far from T_C and agree well with the Skocpol-Beasley-Tinkham (SBT) hotspot model [12]. After the current through the device exceeds the superconducting critical current I_C , circuit-controlled relaxation oscillations are observed until, with increasing voltage, the circuit switches along the load line to the hotspot plateau. Finally, at high voltages, the extension of the hotspot approaches the total length of the nanowire and does not grow any further, so ohmic behavior is observed. The critical current density J_C was estimated from the measured value of I_C and the entire geometrical cross-section of the meander. J_C at 4.2K varied in the 2-4 MA/cm² range, which is a state of the art value.

The ten devices which showed the highest J_C in each chip were mounted on a cryogenic dipstick and optically tested in an liquid He bath at 4.2K. This selection criterion relies on the fact that the most constricted segment of a nanowire determines its I_C . Devices with a constriction (which show a low I_C) are biased well below J_C in most of the meander length, and thus they have a lower quantum efficiency (QE). Bias current was supplied through the DC port of a 10MHz-4GHz bandwidth bias-T connected to the voltage bias circuit already

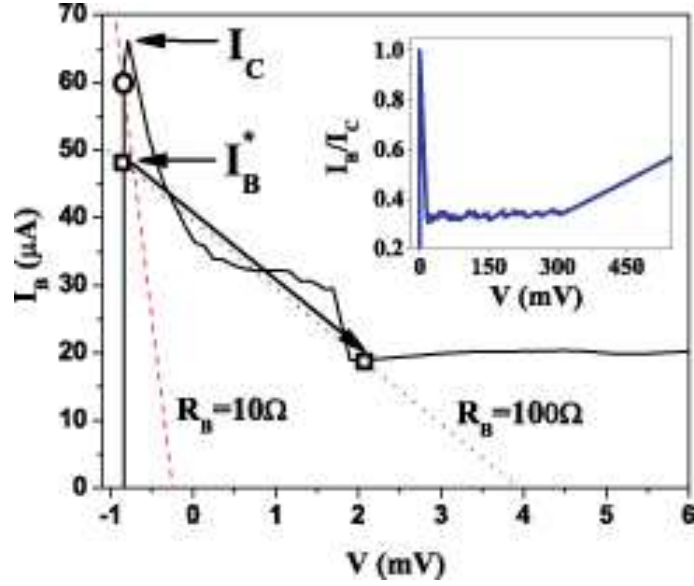


Fig. 3. I-V curve at 4.2K of a 100nm wide, 7nm thick meander (solid line) measured with $R_B = 10\Omega$. For $R_B = 10\Omega$, the DC load line (dashed) never intersects the I-V both in the superconducting and hotspot plateau regions, which is not the case for higher values of R_B (dotted line, for $R_B = 100\Omega$). The voltage offset is due to thermoelectric effects (electrical contact from room temperature to the device is realized through junctions between different metals at different temperatures, so a voltage is created due to the Seebeck effect). The inset shows the I-V curve in a wider voltage range.

described, avoiding the latching effects associated with the current bias. The value for the bias resistor ($R_B = 10\Omega$) was chosen to attain the highest value for the bias current I_B with respect to critical current I_C (dashed line in Fig. 3). Increasing R_B , the noise on I_B due to the voltage source is reduced, but the DC load line (dotted line) become less steep. Consequently, for a given bias current $I_B^* < I_C$ it may intersect the I-V at two points, in the superconducting region and in the hotspot plateau, so that the device permanently switches from the superconducting to the dissipative state. The AC port of the bias-T was connected through a 4dB attenuator to the series of two 18dB gain, 20MHz-3GHz bandwidth, low-noise amplifiers. The amplified signal was then fed to either a 1GHz bandwidth fast oscilloscope for time resolved measurements or a 300MHz counter for statistical analysis. The devices were optically probed using 50ps wide, 25MHz repetition rate pulses at $1.3\mu\text{m}$ wavelength from a fiber-pigtailed, gain-switched laser diode. The photons were fed to the SSPDs through a single-mode optical fiber coupled with a 3mm focal length aspheric lens, which was placed 7cm from the plane of the chip in order to insure uniform illumination of the devices. The average number of incident photons per optical pulse was estimated to be ~ 0.5 with an error of 5%.

The dependence of the number of detector counts per second on the average number of photons per pulse was investigated. As expected [13], the dependence was linear for the photon fluxes used in QE measurements, proof that true single photon detection was observed. Dark counts rate DK was determined as the number of counts registered in one second when the SSPD optical input was blocked. QE at a certain bias current I_B was calculated as: $QE = (N_c - DK)/N_{ph}$, where N_c is the number of detection events registered by the counter in one second, N_{ph} is the number of photons incident on the device area in the same time and DK is

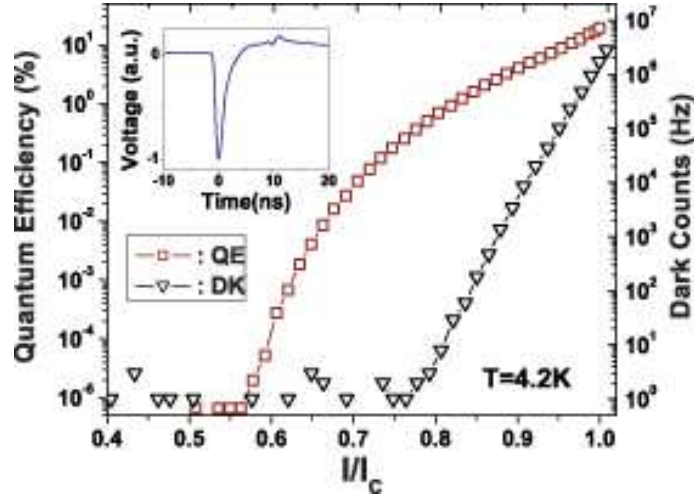


Fig. 4. QE (open squares) and DK (open triangles) as a function of the normalized bias current for the single photon detection regime of an optimum $5 \times 5 \mu\text{m}$ SSPD: $w=100\text{nm}$, $f=40\%$ $t=4\text{nm}$. The incident photon wavelength was $1.3 \mu\text{m}$. Temperature was 4.2K

the dark counts rate at I_B . The best performance was exhibited by a $w=100\text{nm}$, $f=40\%$, $t=4\text{nm}$ meander, which reaches $QE=20\%$ for $1.3 \mu\text{m}$ wavelength light (Fig. 4) before saturation. Using QE and DK from Fig. 4, noise equivalent power (NEP , [14]) was estimated to be of the order of $10^{-16} \text{W}/\text{Hz}^{1/2}$, which is a state of the art value at the temperature of the experiment. This is the best reported result for an SSPD detecting infrared light at 4.2K . We note that a higher QE and a much lower DK may be obtained by cooling the device down to 2K [3]. The time resolved response pulse of our best SSPD showed a full width at half maximum (FWHM) as low as 1.6ns (inset Fig. 4). No degradation in the performance was observed during the measurement period of about one month.

4. Conclusions

The low-temperature fabrication process has been performed also on ultrathin NbN films deposited on GaAs. The electrical and optical measurements, which will be reported elsewhere, are very encouraging for the further developments of the technology on GaAs, allowing for instance monolithic integration with microcavities and waveguides. In conclusion, these results show that high performance NbN SSPDs can be realized on a different substrate and deposited at lower temperature than previously reported, which opens the way to integration with advanced optical structures.

5. Acknowledgments

This work was supported by: Swiss National Foundation through the "Professeur borsier" and NCCR Quantum Photonics program, FP6 STREP "SINPHONIA" (contract number NMP4-CT-2005-16433), IP "QAP" (contract number 15848). The authors thank B. Dwir and H. Jotterand for technical support and useful discussion, Prof. G. Chapuis and N. Guiblin for X-ray diffraction analysis and the Interdisciplinary Centre for Electron Microscopy (CIME) for supplying TEM and SEM facilities.